ORIGINAL ARTICLE

Analysis of a Dual Recuperated Dual Expansion Supercritical CO₂ Cycle for Waste Heat Recovery Applications

Syed J. Hoque[1] · Pramod Kumar[1]

Abstract

Superior performance and compactness of supercritical CO₂ power cycles are encouraging researchers to explore them for waste heat recovery (WHR) applications. This paper presents a comprehensive thermodynamic analysis of a dual recuperated dual expansion cycle utilizing industrial waste heat. The proposed cycle incorporates two recuperators and two turbines with a single compressor. The influence of operating parameters concerning cycle performance in the context of a WHR cycle is discussed. The low side, high side pressures, and the split ratio between the high-temperature and low-temperature turbines are optimized for maximum power rather than thermodynamic cycle efficiency. The cycle performance is evaluated with air as the primary heat transfer fluid in the waste heat recovery heat exchanger operating at a maximum source temperature of 500 °C. The sink temperature is assumed to be 40 °C to enable operation in tropical conditions like India. The paper also compares the performance of the proposed WHR cycle with the baseline single recuperated sCO₂ cycle operating under similar conditions. The analysis shows that the proposed cycle is able to extract 60% more heat and produce 37% more power than the single recuperated sCO₂ cycle. The maximum heat recovery factor for the analyzed WHR cycle is 17.4%, compared to 12.7% for the single recuperated sCO₂ cycle.

Keywords sCO₂ · Waste heat recovery · Split ratio · Heat recovery effectiveness · Cycle efficiency

List of symbols

Acronyms

sCO₂	Supercritical CO₂
WHR	Waste heat recovery
HT	High temperature
LT	Low temperature
DRDE	Dual recuperated dual expansion
SR	Single recuperated

Parameters/variables

$\bar{C}_p$	Average specific heat (kJ/kg.K)
p	Pressure (bar)
T	Temperature (°C)
$\dot{m}$	Mass flow rate (kg/s)
h	Specific enthalpy
$\dot{Q}$	Heat transfer rate (kW)
$\dot{W}$	Power (kW)
p_r	Compressor pressure ratio

x	Split ratio
Δp	Pressure drop (bar)
ΔT_p	Pinch temperature (°C)
λ	Heat recovery factor
η	Efficiency/isentropic efficiency
ε	Heat recovery effectiveness

Subscripts

amb	Ambient
HTT	High-temperature turbine
LTT	Low-temperature turbine
RHT	HT recuperator
RLT	LT recuperator
op	Optimal
exh,i	Exhaust in
exh,o	Exhaust out
in	Recovered
avl	Available
rej	Rejection
s	Isentropic
th	Thermal
max	Maximum
com	Compressor
exh	Exhaust

✉ Pramod Kumar
  pramod@iisc.ac.in

1 Department of Mechanical Engineering, Indian Institute of Science, Bangalore 560 012, India

CO$_2$ Carbon-di-oxide
1–12   Thermodynamic states in the cycle

Introduction

Supercritical CO$_2$ (sCO$_2$) has the potential to replace steam or air as the working fluid for thermal power plants. Besides being inexpensive, CO$_2$ is non-flammable, non-toxic, and less corrosive at high temperatures (Lee et al. 2014) with low environmental impact. Unlike water, CO$_2$ has a significantly lower critical temperature of 31.1 °C and critical pressure of 73.8 bar, respectively. CO$_2$ when compressed to its supercritical state, exhibits excellent heat transfer properties and chemical stability over a wide range of pressures and temperatures. sCO$_2$ being a highly dense fluid, the component sizes are much smaller compared to a similar capacity steam power plant (Yoon et al. 2012). Ahn et al. (2015) compared the efficiencies of various power cycles with different working fluids and concluded that sCO$_2$ based power cycles are more efficient than other cycles at temperatures greater than 500 °C. Nearly four decades back, in Feher (1968) proposed the first sCO$_2$ based power cycle for space exploration. Subsequently, there has been renewed interest with a significant work on cycle optimization by Angelino (1968) and Dostal et al. (2004). Presently sCO$_2$ cycles are actively being researched to explore applications such as nuclear power plants (Moisseytsev and Sienicki 2009; Ahn and Lee 2014), concentrated solar power plants (Neises and Turchi 2014), fossil fuel power plants (Moullec 2013; Johnson et al. 2012), and waste heat recovery plants (Us 2013). The simplest sCO$_2$ power cycle is the single recuperated Brayton cycle comprising a single recuperator, gas cooler, turbine, and compressor. Unlike conventional Rankine or air

Brayton cycles, all sCO$_2$ cycles are heavily recuperated. The unique thermodynamic property of sCO$_2$ allows for near isothermal expansion across the turbine with the enthalpy drop primarily governed by the pressure ratio. The recuperated heat from the turbine exhaust is used to preheat the working fluid before it enters the heater, thereby contributing to the increased cycle efficiency of a sCO$_2$ power plant.

Waste heat is the heat generated by thermodynamic systems such as gas turbine power blocks or from industrial processes, which if unutilized is rejected to the ambient. Waste heat is generated as a byproduct of process industries such as steel, glass, aluminium, or petrochemical refineries or from the exhaust of gas turbines producing power by burning fossil fuels. The quantum of waste heat is continually rising due to increasing industrialization. Waste heat is generally categorized depending on the temperature of the heat source. Figure 1 shows the classification of waste heat generated from typical applications. The literature on waste heat recovery is based on the temperature of heat available; Forman et al. (2016) estimated waste heat potential at 300 °C, Papapetrou et al. (2018) at 500 °C, Vance et al. (2019) at 650 °C. A common outcome from the investigations suggests that more than 40% of wasted energy can be potentially recovered by a suitable waste heat recovery cycle to improve the exergetic efficiency of the system or process. Unlike a conventional power cycle where heat addition ideally occurs without a drop in the source temperature, in a waste heat recovery (WHR) cycle the heat source temperature continually decreases on account of heat extraction in the recovery heat exchanger. The maximum quantity of extractable heat depends on the source temperature and the inlet temperature of the working fluid entering the recovery heat exchanger. Preheating the working fluid before the recovery heat exchanger is undesirable as it increases
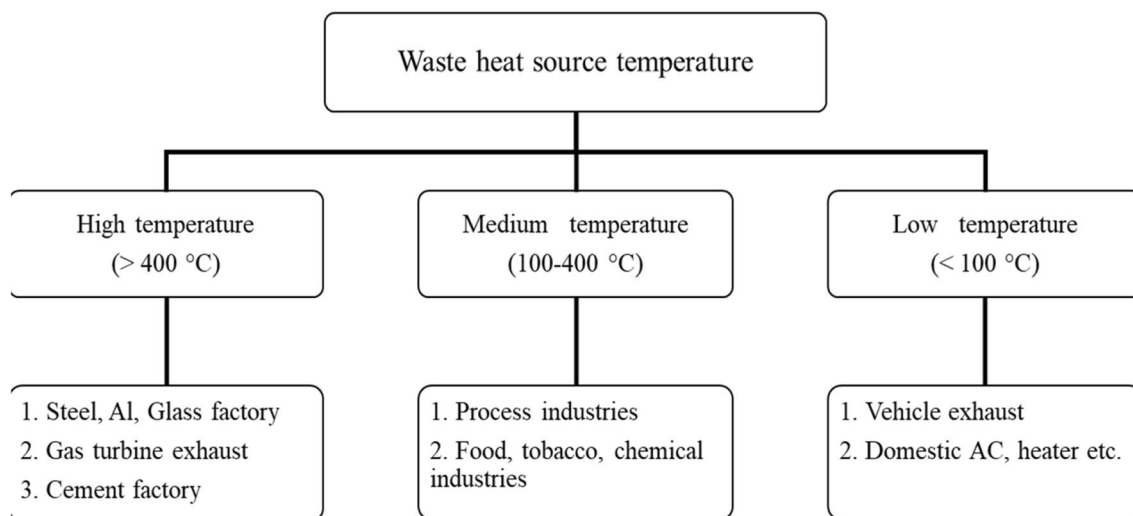

Fig. 1 Classification of waste heat based on source temperatures

the inlet temperature of the working fluid, thus limiting the quantum of heat extracted from the source. In this aspect, the highly recuperated sCO_2 cycle is not an ideal choice for a WHR cycle.

sCO_2 Cycles for Waste Heat Recovery applications

Several sCO_2 cycle configurations for WHR applications have been proposed in the literature (Mohagheghi and Kapat 2013; Kimzey 2012; Cho et al. 2015; Wu 2016; Huck et al. 2016; Sen Wang et al. 2018; Kim et al. 2016; Olumayegun and Wang 2019). The common layouts suggested are recompression, partial heating, pre-compression, split-flow, dual heated cascade, dual expansion cycles. Mohagheghi and Kapat (2013) worked on a single recuperated and recompression WHR cycles. These cycles were optimized for maximum power output in the temperature range of 230–830 °C. Kimzey (2012) proposed three novel WHR cycles by the splitting flow between two turbines operating at different temperatures. These cycles were analyzed for heat recovery from a gas turbine exhaust with varying exhaust temperatures. The author concluded that these novel cycles outperform two-pressure level steam cycles but underperform when compared with a three-pressure level reheat steam cycle operating under identical conditions. In a similar study, Cho et al. (2015) analyzed recompression, dual heated, dual expansion WHR cycles for gas turbine exhaust. They compared these cycles with the novel sCO_2 cycles proposed by Kimzey (2012) and reported contrasting results. The analysis showed that advanced cycle layouts comprising of dual split-flow outperform the triple-pressure reheat steam cycle. Subsequently, many other authors (Wu 2016; Huck et al. 2016) explored single recuperated, dual recuperated, triple recuperated, dual split flow, and dual expansion cycles for other WHR applications. The performance of these cycles in comparison with steam has been reported in Sen Wang et al. (2018), Kim et al. (2016), Olumayegun and Wang (2019). The extensive work on WHR cycles by these authors suggest that the choice of the cycle is specific to operating conditions and the nature of the waste heat source. Commercialization of sCO_2 based WHR cycle up to 30 MW (Held 2015) by Echogen (OH, USA) (Us 2013; Incorvia 2015) and General Electric (NY, USA) (Incorvia 2015) is also documented in the literature.

The dual recuperated dual expansion (DRDE) sCO_2 cycle, proposed by Kimzey (2012), is found to be a promising contender for WHR applications. An identical cycle, referred to as the single heated cascade cycle, has been analyzed by Kim et al. (2016) as a potential exhaust heat-driven bottoming cycle for a gas turbine. A cycle thermal efficiency of 27.3%, corresponding to a turbine inlet temperature of 493 °C was reported. Subsequently, Manente and Costa (2019) conducted a detailed analysis of the DRDE cycle

and projected a heat recovery factor of 14.18% and cycle thermal efficiency of 16.93%, at a turbine inlet temperature of 500 °C. The analysis accounted for variable turbine inlet temperatures with fixed operating pressures.

Objective of the Present Paper

This paper presents a comprehensive analysis of the dual recuperated dual expansion sCO_2 WHR cycle. Although many authors have evaluated the DRDE sCO_2 cycle for WHR applications, the major limitation in the reported literature is the assumption of fixed high-side and low side pressures. This paper aims to fill this lacuna by presenting a focused, systematic thermodynamic assessment of the DRDE sCO_2 WHR cycle accounting for the variation in cycle pressures. The analysis identifies various operating parameters that affect the performance of the DRDE WHR cycle. Subsequently, the influences of each parameter on the specific objective of maximizing heat recovery and work output are analyzed in detail to gain insights into the off-design performance of the cycle. Finally, the performance of the optimized DRDE WHR cycle is compared with the baseline single recuperated sCO_2 cycle operating under optimized conditions.

Dual Recuperated Dual Expansion sCO_2 WHR Cycle

A DRDE WHR cycle has the potential to extract a higher amount of heat from the waste heat source than most other sCO_2 cycle configurations. A drawback of the DRDE cycle is the inherently complex thermodynamic cycle associated with increased system components. Unlike a single recuperated (SR) sCO_2 cycle consisting of one compressor, one turbine, and three heat exchangers, a DRDE WHR cycle employs a single compressor, a set of high and low-temperature turbines, and four heat exchangers as shown in Fig. 2.

The corresponding temperature-entropy (T-s) diagram of the DRDE WHR cycle is shown in Fig. 3. Internal heat recuperation by HT Recuperator and LT Recuperator are marked as $\dot{Q}_{RHT}$ and $\dot{Q}_{RLT}$, respectively. HT stream massflow rate ($\dot{m}_{HT}$) and LT stream massflow rate ($\dot{m}_{LT}$) are represented by dashed and dotted lines, respectively.

Description of the Thermodynamic Model

Objective Function for a WHR Cycle

Contrary to a standard power cycle, where efficiency is the principal driver, a WHR cycle is designed to maximize the work output from the available heat. Therefore, the objective
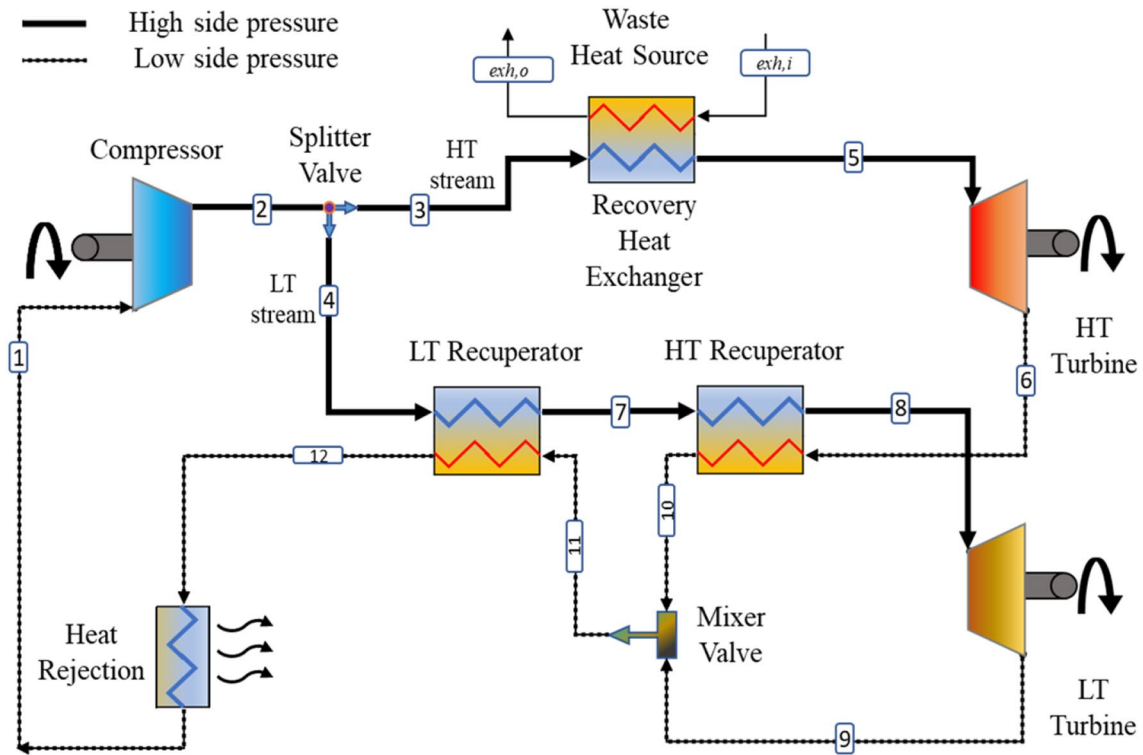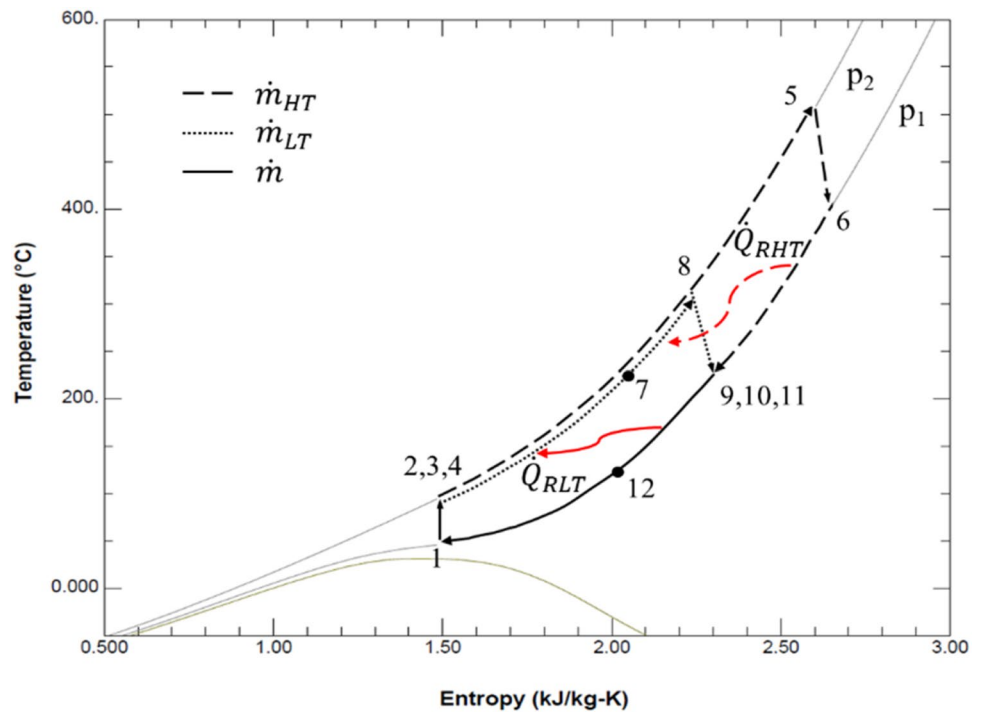
Fig. 2 Thermodynamic representation of dual recuperated dual expansion sCO_2 WHR cycle with components

Fig. 3 T-s diagram for the DRDE-WHR cycle

function for a WHR significantly influences the design of the thermodynamic cycle. The performance of a conventional power generation cycle is measured by the thermal efficiency (η_{th}), whereas, the performance of a WHR cycle is measured by heat recovery factor (λ) (Manente and Costa 2019). Heat

recovery factor (λ) is defined as the ratio of net power output ($\dot{W}_{net}$) to available heat ($\dot{Q}_{avl}$).

$$\lambda = \frac{\dot{W}_{net}}{\dot{Q}_{avl}} \qquad (1)$$

Available heat is estimated considering the potential temperature differential between waste heat exhaust temperature ($T_{exh,i}$) and the ambient temperature (T_{amb}).

$$\dot{Q}_{avl} = \dot{m}_{exh}\bar{C}_p(T_{exh,i} - T_{amb}) \qquad (2)$$

Equation 2 provides the thermodynamic limit of heat extraction; however, in most practical cases, it is possible to extract only a part of the available heat from the heat source, which is termed as the recovered heat ($\dot{Q}_{in}$).

$$\dot{Q}_{in} = \dot{m}_{exh}\bar{C}_p(T_{exh,i} - T_{exh,o}) \qquad (3)$$

The ratio of recovered heat to available heat is known as heat recovery effectiveness (ε).

$$\varepsilon = \frac{\dot{Q}_{in}}{\dot{Q}_{avl}} \qquad (4)$$

Heat recovery effectiveness is a useful parameter for evaluating the performance of a WHR cycle as it is a measure of waste heat recovered by the cycle. The thermal efficiency of a WHR cycle is the ratio of net power output to recovered heat.

$$\eta_{th} = \frac{\dot{W}_{net}}{\dot{Q}_{in}} \qquad (5)$$

Hence, heat recovery factor (λ) can be written as the product of heat recovery effectiveness and thermal efficiency.

$$\lambda = \eta_{th}\varepsilon \qquad (6)$$

Analysis of the DRDE sCO$_2$ WHR Cycle

This section presents the governing equations for the DRDE-WHR sCO$_2$ cycle. Hereafter, in the subsequent sections of the paper, for brevity, the DRDE-WHR sCO$_2$ cycle will be simply referred to as the WHR cycle. As the name suggests, it is important to mention that the WHR cycle always operates in the supercritical state above the critical point of CO$_2$. Referring to cycle schematic Fig. 2 and corresponding T-s diagram in Fig. 3, supercritical CO$_2$ at *state 1* is compressed to *state 2* using a compressor. Isentropic efficiency of the compressor is defined as

$$\eta_{com} = \frac{h_{2s} - h_1}{h_2 - h_1} \qquad (7)$$

The high-pressure CO$_2$ leaving the compressor (at *state 2*) is divided into two streams, viz. high temperature (HT) stream (*state 3*) and low temperature (LT) stream (*state 4*), using a splitter valve.

$$\dot{m} = \dot{m}_{HT} + \dot{m}_{LT} \qquad (8)$$

Split ratio (x) is defined as the ratio of HT stream massflow rate ($\dot{m}_{HT}$) to total massflow rate ($\dot{m}$).

$$x = \frac{\dot{m}_{HT}}{\dot{m}} \qquad (9)$$

HT stream (at *state 3*) is circulated through the waste recovery heat exchanger, where heat is transferred from the waste heat source to the WHR cycle (state 3–5).

$$\dot{Q}_{in} = \dot{m}_{HT}(h_5 - h_3) \qquad (10)$$

The average temperature of the HT stream is higher compared to the LT stream as heat addition occurs solely in the HT stream. The hot HT stream at state 5 is expanded in a high-temperature (HT) turbine to state 6.

$$\eta_{HTT} = \frac{h_5 - h_6}{h_5 - h_{6s}} \qquad (11)$$

Alternatively, the LT stream at state 4 is circulated through two recuperators (HT Recuperator and LT Recuperator) to facilitate heat addition before being expanded in a low-temperature (LT) turbine from state 8 to state 9.

$$\eta_{LTT} = \frac{h_8 - h_9}{h_8 - h_{9s}} \qquad (12)$$

The hot stream leaving the HT turbine is passed through the HT recuperator at state 6 to heat the LT stream leaving the LT recuperator at state 7.

$$\dot{Q}_{RHT} = \dot{m}_{HT}(h_6 - h_{10}) = \dot{m}_{LT}(h_8 - h_7) \qquad (13)$$

Subsequently, the stream leaving the HT recuperator at state 10 is combined with the LT turbine exhaust at state 9 into a single stream using a mixing valve. It may be noted that the mixing of streams at states 9 and 10 occurs at identical pressures and temperatures ($T_9 \approx T_{10}$). The DRDE cycle is constrained to ensure constant pressure and constant temperature mixing from states 9 and 10. The pressure constraint is satisfied by the inherent cycle configuration, whereas the temperature constraint is achieved by a judicial split of the mass flow at the compressor exit. The unified stream leaving the mixing valve at state 11 is passed through the LT recuperator to preheat the LT stream leaving the splitter valve.

$$\dot{Q}_{RLT} = \dot{m}(h_{11} - h_{12}) = \dot{m}_{LT}(h_7 - h_4) \qquad (14)$$

Residual heat is then rejected to the ambient using a suitable heat exchanger from state 12 to state 1.

$$\dot{Q}_{rej} = \dot{m}(h_{12} - h_1) \tag{15}$$

The cold stream leaving the heat exchanger is circulated back to the compressor inlet, thus completing the cycle.

Pressure ratio (p_r) across the compressor is the ratio of outlet pressure (p_2) to inlet pressure (p_1) and is defined as

$$p_r = \frac{p_2}{p_1} \tag{16}$$

Exhaust gas pressure is assumed to be fixed at 1.02 bar for this study.

WHR Cycle Operating Conditions

The operating envelope and limits for the WHR cycle are listed in Table 1. Source of waste heat is considered to be at a temperature of 500 °C, which is typical of a gas turbine exhaust or industrial heat from steel and cement plants. The composition of gas turbine exhaust is idealized to be air for the purpose of analysis. Ambient temperature (T_{amb}) is assumed to be 40 °C considering tropical climatic conditions. The exit temperature of CO_2 leaving the gas cooler is assumed to be 5 °C higher than the ambient temperature to facilitate heat rejection. As a result, for an ambient of 40 °C, the compressor inlet temperature is fixed at 45 °C in this study. The isentropic efficiency of the compressor is assumed to be 75%, as reported in (Lee et al. 2018; Garg et al. 2015). Generally, the turbines are known to have slightly better isentropic efficiencies (Garg et al. 2015; Xia et al. 2019; Qi et al. 2017), hence the isentropic efficiency for the turbine is assumed to be 80%. Apart from operating

conditions, isentropic efficiencies of turbomachinery are influenced by power generation capacity, type of turbomachinery (axial or radial) and off-design or part load operation (Sathish et al. 2021; Samad et al. 2020). The pressure drop across heat exchangers is assumed to be 2% of the inlet pressure (Pandey et al. 2020; Khadse et al. 2018). Pinch temperature split across all heat exchanging devices is assumed to be 5 °C, a standard practice for supercritical CO_2 power generation systems (Samad et al. 2020; Pandey et al. 2020).

Influence of Cycle Parameters on Objective Function

Heat recovery factor (λ) of the WHR cycle depends on operating parameters presented in Table 1. There are two types of operating parameters, fixed parameters are constant throughout the study, whereas variable parameters can be varied within the specified limits to optimize the cycle performance. Referring to the WHR cycle in Figs. 2 and 3, heat recovery factor is expressed as

$$\lambda = f(\dot{m}_{exh}, T_{exh,i}, p_1, p_2, \dot{m}_{HT}, \dot{m}_{LT}) \tag{17}$$

Out of the six parameters, exhaust gas massflow rate ($\dot{m}_{exh}$) and exhaust gas temperature ($T_{exh,i}$) are dictated by the external heat source and hence, cannot be controlled by the WHR. Since, $T_{exh,i}$ becomes a fixed parameter, therefore, the resulting cycle massflow rate ($\dot{m}_{HT}$) for CO_2 is calculated on the unit basis of exhaust flow rate ($\dot{m}_{exh}$). Heat recovery factor now can be reduced to a function of four operating parameters.

$$\lambda = f(p_1, p_2, \dot{m}_{HT}, \dot{m}_{LT}) \tag{18}$$

For every pair of p_1 and p_2, there are optimal values of $\dot{m}_{HT}$ and $\dot{m}_{LT}$ for which λ attains a maximum value.

Table 1 WHR Operating parameters, type, and value

Operating parameter	Parameter type	Symbol	Unit	Value/range
Exhaust gas composition	Fixed	–	–	Air
Exhaust gas temperature	Fixed	$T_{exh,i}$	°C	500
Exhaust gas pressure	Fixed	$p_{exh,i}$	bar	1.02
Ambient temperature	Fixed	T_{amb}	°C	40
Compressor inlet temperature	Fixed	T_1	°C	45
Compressor inlet pressure	Variable	p_1	bar	75–600
Compressor outlet pressure	Variable	p_2	bar	75–600
HT stream massflow rate	Variable	$\dot{m}_{HT}$		Calculated
LT stream massflow rate	Variable	$\dot{m}_{LT}$		0–100 per unit $\dot{m}_{exh}$
Isentropic efficiency of compressor	Fixed	η_{com}	%	75
Isentropic efficiency of HT turbine, LT turbine	Fixed	η_{HTT}, η_{HTT}	%	80
Pressure drops in heat exchanger, recuperators, and gas cooler	Fixed	$\frac{\Delta p}{p}$	%	2
Pressure drop across pipes	Fixed	Δp	%	0
Pinch temperature of heater, recuperators, and gas cooler	Fixed	ΔT_p	°C	5

$$\lambda_{\text{op}} = f(p_1, p_2, \dot{m}_{\text{HT,op}}, \dot{m}_{\text{LT,op}}) \tag{19}$$

Optimal HT Massflow Rate ($\dot{m}_{\text{HT,op}}$)

Heat recovery factor (λ) of the WHR cycle is the product of ε and η_{th}. The maximum value of λ can be achieved for a particular values of ε and η_{th}. HT stream massflow rate ($\dot{m}_{\text{HT}}$), and the split ratio plays a vital role in overall WHR cycle performance. The optimal value of ε and η_{th} are highly dependent on the $\dot{m}_{\text{HT}}$. Figure 4 shows the schematic of the recovery heat exchanger between the waste heat source and the WHR cycle.

For a fixed value of exhaust gas massflow rate ($\dot{m}_{\text{exh}}$) and exhaust gas temperature ($T_{\text{exh},i}$), if $\dot{m}_{\text{HT}}$ is insufficient, then heat recovery effectiveness would attain a lower value. However, the inlet temperature of the HT turbine (T_5) would reach a maxima. On the other hand, a high $\dot{m}_{\text{HT}}$ would decrease the inlet temperatures of both HT and LT turbines. Nevertheless, heat recovery effectiveness would still be maximum in this case. Thermodynamically, thermal efficiency (η_{th}) of a cycle depends on the turbine inlet temperature. Higher inlet temperatures lead to higher η_{th}. Therefore, higher values of $\dot{m}_{\text{HT}}$ would tend to subdue η_{th} of a WHR cycle. Referring to Fig. 4, the heat recovered by sCO$_2$ stream is

$$\dot{Q}_{\text{in}} = \dot{m}_{\text{HT}}(h_5 - h_3) \tag{20}$$

Similarly, heat transferred by the air stream from the waste heat source is

$$\dot{Q}_{\text{in}} = \dot{m}_{\text{exh}}(h_{\text{exh},i} - h_{\text{exh},o}) \tag{21}$$

Combining Eqs. 20 and 21, HT stream massflow rate is expressed as

$$\dot{m}_{\text{HT}} = \frac{\dot{m}_{\text{exh}}(h_{\text{exh},i} - h_{\text{exh},o})}{(h_5 - h_3)} \tag{22}$$

The specific enthalpy of fluid is function of temperature and pressure,

$$h = f(T, p) \tag{23}$$

For a maximum ε, the exhaust gas outlet temperature of the recovery heat exchanger is,

$$T_{\text{exh},o} = T_3 + \Delta T_p \tag{24}$$

where, ΔT_p is the pinch temperature of the recovery heat exchanger. On the other hand, the inlet temperature of the HT turbine (T_5) needs to be as high as possible for maximizing η_{th} of the WHR cycle. The maximum achievable value of T_5 is,

$$T_5 = T_{\text{exh},i} - \Delta T_p \tag{25}$$

The optimal value HT stream massflow rate ($\dot{m}_{\text{HT,op}}$) corresponds to conditions satisfied by Eqs. 24 and 25, following which, the optimal value of HT stream massflow is expressed as

$$\dot{m}_{\text{HT,op}} = \frac{\dot{m}_{\text{exh}}\{f(T_{\text{exh},i}, p_{\text{exh},i}) - f(T_3 + \Delta T_p, p_{\text{exh},o})\}}{\{f(T_{\text{exh},i} - \Delta T_p, p_5) - f(T_3, p_3)\}} \tag{26}$$

where the outlet pressures (both exhaust air and sCO$_2$ streams) in the recovery heat exchanger are 2% lower than the corresponding inlet pressures as mentioned in Table 1. $T_{\text{exh},i}$ and $p_{\text{exh},i}$ are assumed as fixed parameters, specific enthalpy values used in Eq. 26 are obtained using REF-PROP® (Lemmon et al. 2020). The optimal HT massflow rate depends on T_3 ($T_3 = T_2$) and p_3 ($p_3 = p_2$), since compressor outlet temperature (T_2) depends on the pressure ratio (p_2/p_1) for a fixed compressor inlet temperature (T_1) and isentropic efficiency (η_{com}). The optimal HT massflow rate,

Fig. 4 Recovery heat exchanger of the WHR cycle
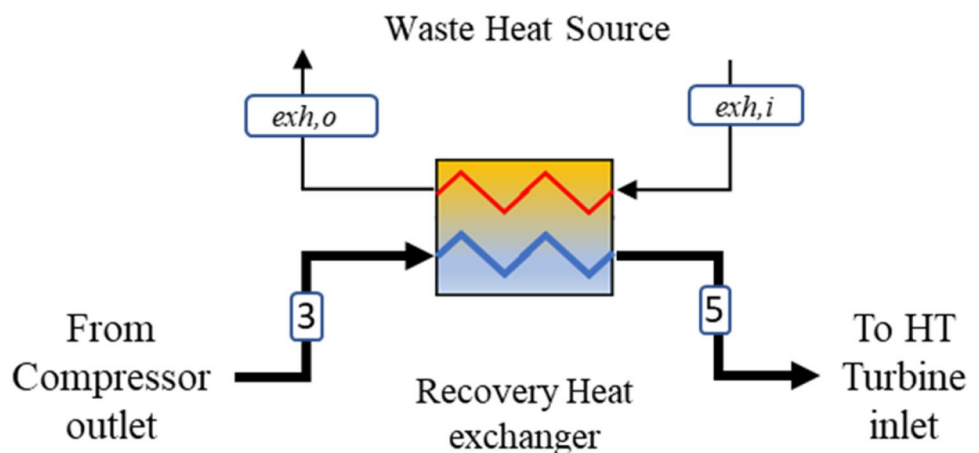
therefore, only depends on compressor inlet pressure (p_1) and outlet pressure (p_2). $\dot{m}_{HT,op}$ is calculated using Eq. 26. The resulting temperature profiles of the hot and cold streams along the length and the location of the pinch in the recovery heat exchanger is shown in Appendix I.

Unfortunately, there is no straight forward way to find the optimal LT massflow rate ($\dot{m}_{LT,op}$), as a result, optimal LT massflow rate is calculated using an iterative procedure as explained in flow chart in Fig. 5.

Description of Thermodynamic Code for Cycle Simulation

An in-house code has been developed for thermodynamic cycle simulation to understand the influence of operating variables. The code is developed in MATLAB® (Inc 2020) and coupled with the REFPROP® (Lemmon et al. 2020) database for updating the thermodynamic data. Pressure drop and temperature pinch data across pipes and heat exchangers are included as input parameters. The algorithm automatically detects the pinch location in the heat exchanger to estimate the quantum of heat transferred accurately. There are two methods of arriving at the optimized operating parameters. A simple straight forward method is to simulate the WHR cycle using a four-variable iterative nested loop, wherein, each variable representing a single operating parameter is independently varied. This approach would result in a four-dimensional matrix, with each dimension uniquely representing a single operating parameter. The code would subsequently solve all possible combinations of input parameters to arrive at optimal values for each parameter. This method, although simple, is computationally expensive. Fortunately, there is an alternative method to find the optimal HT stream massflow rate ($\dot{m}_{HT,op}$) without the need for iterations. This method is explained in Optimal HT Massflow Rate ($\dot{m}_{HT,op}$). Hence, the number of operating parameters is reduced to three, resulting in a computationally frugal three-dimensional matrix. The algorithm used for the thermodynamic code is presented in the flow chart in Fig. 5.

Compressor inlet pressure and outlet pressure is varied from 75 to 600 bar in the present analysis, ensuring that $p_r > 1$ at all conditions. HT stream massflow rate ($\dot{m}_{HT}$) is calculated using Eq. 26. LT stream massflow rate ($\dot{m}_{LT}$) is varied per unit of $\dot{m}_{exh}$. Higher values of $\dot{m}_{LT}$ would lead to negative power output as power consumption by the compressor would be higher than power produced by the turbines.

Results and discussion

The influence of the operating parameters for the DRDE WHR sCO$_2$ cycle is explained using air as the waste heat working fluid in the primary side of the recovery heat exchanger. The results are presented per unit mass flow rate ($\dot{m}_{exh}$) of air flowing through the recovery heat exchanger. In principle, the analysis and methodology presented can be extended to any heat transfer fluid undergoing single-phase heat transfer.

Selection of Optimal Massflow Ratio of HT Stream

Figure 6 shows the effect of HT stream mass flow rate of CO_2 ($\dot{m}_{HT}$) on HT turbine inlet temperature (T_5), and heat recovery effectiveness (ε). The results are obtained for air with a fixed exhaust gas inlet temperature of 500 °C, as stated in Table 1. The values on the x axis are the ratio of $\dot{m}_{HT}$ to exhaust gas flow rate $\dot{m}_{exh}$, the maximum value of mass flow ratio depends on the net enthalpy of the heat transfer fluid. It is observed that heat recovery effectiveness increases linearly with an increase in massflow rate of the HT turbine up to a certain value of mass flow ratio, and thereafter, the heat recovery effectiveness remains constant at a maximum value of 0.91 for a pinch of 5 °C. Similarly, the HT turbine inlet temperature remains constant at 495 °C (5 °C lower than inlet exhaust temperature of 500 °C) up to a specific increase in HT mass flow rate and thereafter, decreases nonlinearly with further increase in HT mass flow. It is interesting to note that the optimal ratio of HT turbine mass flow rate to exhaust mass flow rate with air as the heat transfer fluid (0.74 in this case obtained from Fig. 6) is identical for both heat recovery effectiveness and HT turbine inlet temperature. The reason for such a trend has been explained earlier in Optimal HT Massflow Rate ($\dot{m}_{HT,op}$). A similar trend is obtained for varying high side and low side pressures. Therefore, to estimate the optimal HT mass to exhaust mass fraction, it is sufficient to plot a single variable, i.e., heat recovery effectiveness alone for a range of operating conditions. The value of $\dot{m}_{HT,op}$ is obtained using Eq. 26 and without the need for iterations.

Figure 7 shows the effect of compressor inlet pressure (p_1) on $\dot{m}_{HT,op}$ and ε. In this case, the compressor discharge pressure (p_2) is fixed at 200 bar. A higher compressor inlet pressure reduces the pressure ratio across the compressor leading to a lower discharge temperature (T_2). A lower value of T_2 enhances heat recovery, thus improving the heat recovery effectiveness. In addition, an increase in low side pressure also decreases the optimal mass flow rate to the HT turbine, as observed in Fig. 7. This is on account of a higher temperature differential across the HT stream passing through the recovery heat exchanger resulting in a lower HT turbine mass flow rate for a fixed quantum of available heat.

Extending the analysis, Fig. 8 shows a contour map of the ratio of $\dot{m}_{HT,op}$ to exhaust mass flow rate ($\dot{m}_{exh}$), and corresponding heat recovery effectiveness (ε) for a range of high side and low side pressures. The high side pressure is varied from 75 to 600 bar to understand the effect of the operating
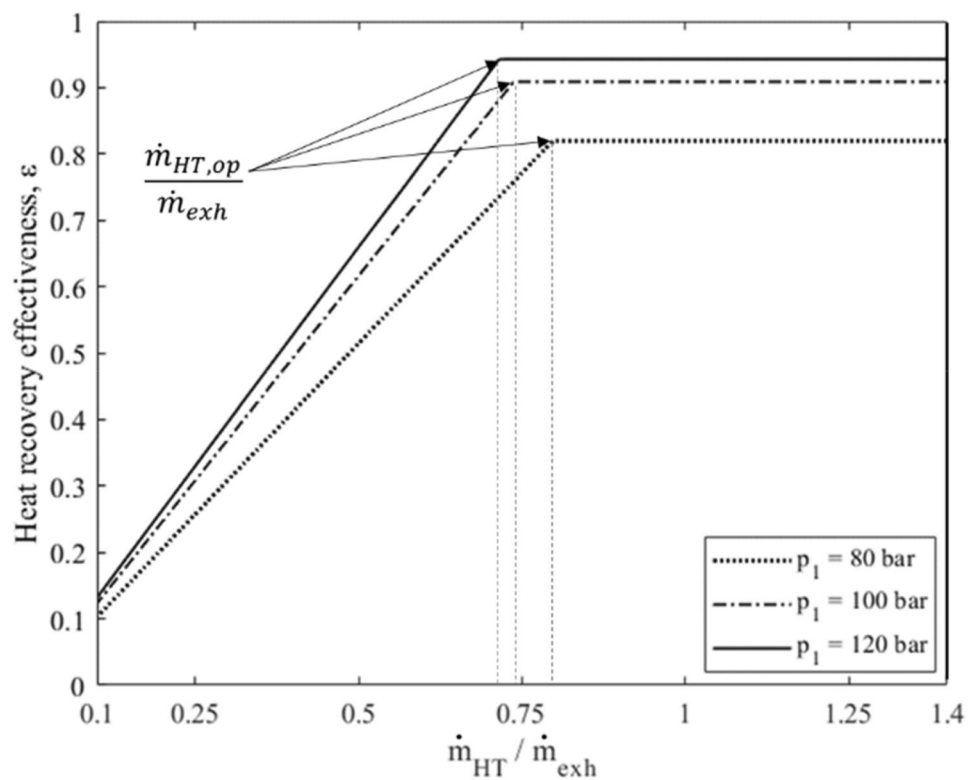
Fig. 5 Flow Chart for thermodynamic simulation of the WHR cycle
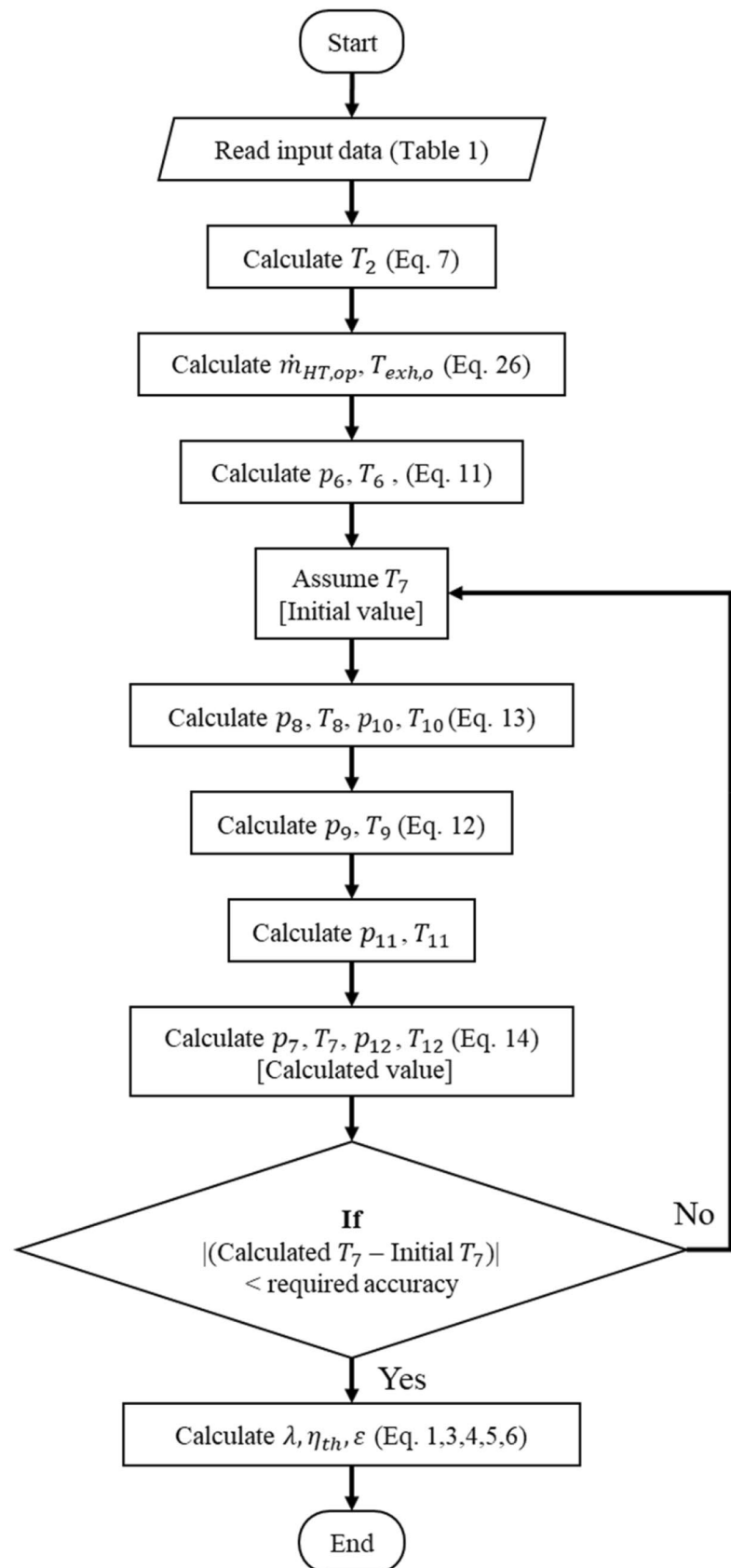
Fig. 6 Effect of HT massflow rate ($\dot{m}_{HT}$) on HT turbine inlet temperature (T_5),and heat recovery effectiveness (ε) for $p_1 = 100$ bar, $p_2 = 200$ bar
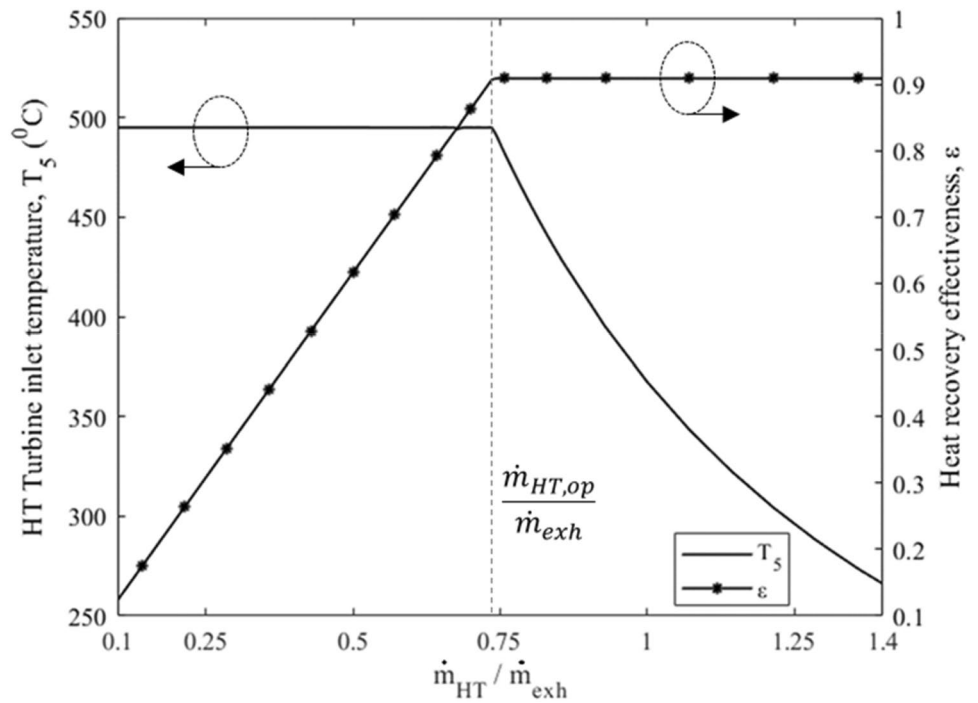
Fig. 7 Effect of low side pressure on optimal mass fraction ratio $\dot{m}_{HT,op}$ and ε for a fixed high side pressure, $p_2 = 200$ bar

pressure ratio. Figure 8 provides some interesting information on the influence of high side pressure on heat recovery effectiveness and optimal HT turbine mass flow rate.

It is found that an increase in high side pressure adversely impacts the heat recovery effectiveness for the entire range of

low side pressures. For example, the maximum heat recovery effectiveness of 0.9 is capped at high side pressure below 280 bar. As explained previously, higher compressor discharge temperature leads to lower heat recovery, and hence, the optimal high side pressure for the WHR cycle is limited to pressure

Fig. 8 Contours of $\dot{m}_{HT,op}$ and corresponding ε for various pressure ratio
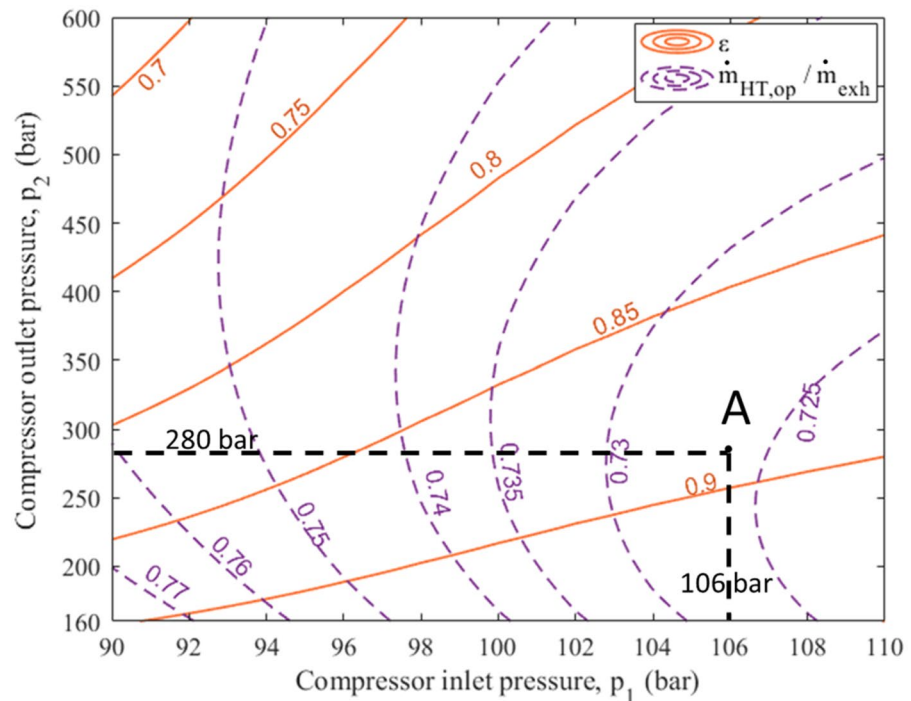
less than 280 bar. The corresponding optimal HT mass flow rate can be obtained by fixing the high and low side pressure for any desired heat recovery effectiveness. It is interesting to note that the optimal HT turbine mass flow rate decreases with increasing compressor inlet pressure for a fixed value to heat recovery effectiveness. This trend is consistent in the results presented in Fig. 7.

Until now, the emphasis was on estimating the optimal mass flow rate and operating pressures across the HT turbine (or the compressor) by maximizing waste heat recovery. It is important to note that the LT stream's massflow rate did not influence the foregoing analysis. Before proceeding further, it is essential to summarize the observations made so far.

1. Optimal HT massflow rate ($\dot{m}_{HT,op}$) is independent of $\dot{m}_{LT}$.
2. Heat recovery effectiveness (ε) is dependent on $\dot{m}_{HT}$, not on $\dot{m}_{LT}$.
3. Optimal HT massflow rate ($\dot{m}_{HT,op}$) and ε are dependent on p_1 and p_2.

In the subsequent section, we turn to focus on arriving at optimal LT turbine mass flow rate ($\dot{m}_{LT,op}$) and maximizing the heat recovery factor (λ). It is done iteratively by the thermodynamic code described by the Flow Chart in Fig. 5.

## Optimal LT Stream Massflow Rate ($\dot{m}_{LT,op}$) and Optimal Heat Recovery Factor (λ_{op})

Optimal heat recovery factor (λ_{op}), is the highest value of λ for any low and high side pressures p_1 and p_2, respectively. The values of $\dot{m}_{HT}$ and $\dot{m}_{LT}$ corresponding to optimal heat recovery factor are denoted by $\dot{m}_{HT,op}$ and $\dot{m}_{LT,op}$. The procedure for obtaining the optimal value of HT mass flow rate ($\dot{m}_{HT,op}$) has been explained previously in Optimal HT Massflow Rate ($\dot{m}_{HT,op}$).

Figure 9 presents a contour map of λ_{op}, for a range of compressor inlet and outlet pressures for the cycle conditions listed in Table 1. The corresponding values of optimal HT turbine mass flow rate ($\dot{m}_{HT,op}$) and heat recovery effectiveness (ε) are obtained from Fig. 8.

For the present cycle operating conditions, the maximum value of optimal heat recovery factor ($\lambda_{op,max}$) is found to be 0.174, denoted by point 'A' in Fig. 9. The corresponding pressures, p_1 and p_2 are found to be 106 and 280 bar, respectively. Referring back to Fig. 8, it is observed that the location of $\lambda_{op,max}$ (point 'A') does not correspond to the maximum effectiveness value of 0.9 for a compressor discharge pressure of 280 bar and an inlet temperature of 106 bar. Besides, point 'A' does not coincide with the lowest optimal HT turbine mass flow rate as well. This suggests
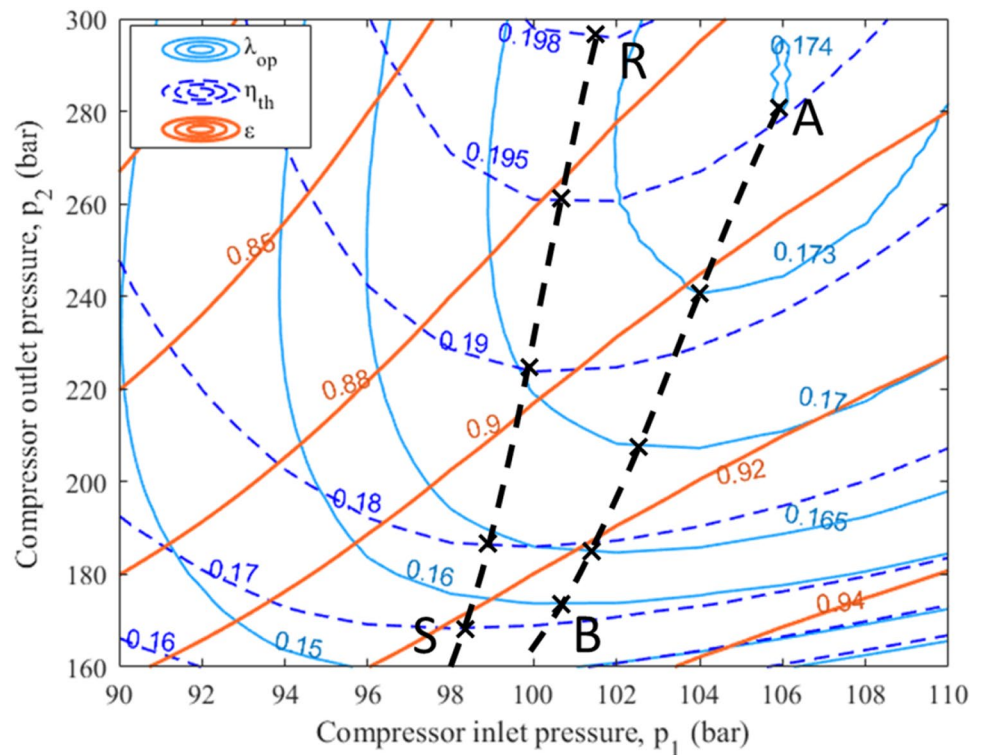
Fig. 9 Contour of λ_{op} of WHR cycle for various p_1 and p_2
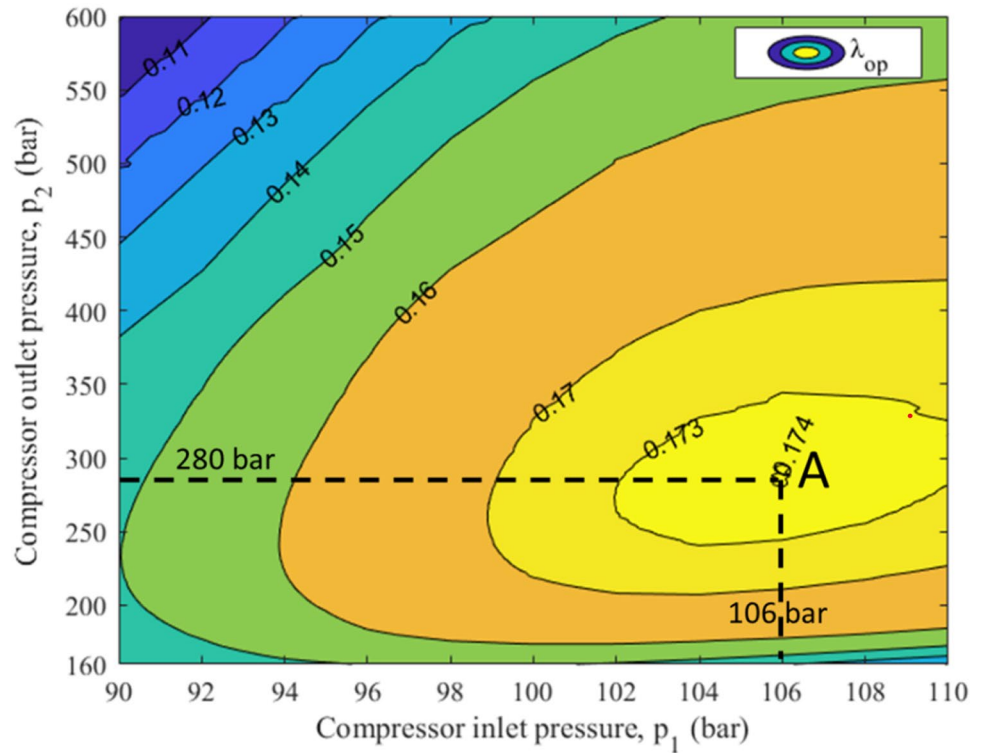
that there is a tradeoff between the heat recovery effectiveness, compressor inlet, outlet pressures, and optimal HT turbine mass flow rate that maximizes λ. This aspect is further explored in Fig. 10.

Fig. 10 Contours of λ_{op}, η_{th} and ε for different compressor inlet and outlet pressures

In the results presented in Fig. 10, the maximum value of high side pressure is capped at 280 bar, corresponding to the $\lambda_{op,max}$ value of 0.174 (point 'A'). The reader may note that the location of $\lambda_{op,max}$ is corresponds to $\varepsilon \sim 0.89$ and $\eta_{th} \sim 0.195$. However, the values do not coincide with the local maxima of either ε or η_{th}. The highest thermal efficiency for the cycle occurs at a much higher pressure than the optimal heat recovery factor.

Selection of WHR Cycle "Design-Point"

A closer observation of both the optimal heat recovery factor (λ_{op}) and cycle thermal efficiency (η_{th}) in Fig. 10, reveals a parabolic behavior. The vertices of the λ_{op} and η_{th} depict a minima in compressor discharge pressure. Lines A-B and R-S in Fig. 10 are the loci of the vertices of the parabolic curves of λ_{op} and η_{th}. Points on lines A-B and R-S provide the corresponding maximum values of λ_{op} and η_{th} achievable at lowest high side pressure. Since the goal of a WHR system is to maximize the heat recovery factor, therefore, the preferred operating point would lie on the line of A-B and not on R-S. Depending on the allowable high side pressure of the system (from the perspective of stress analysis, material, and manufacturing limitations), a suitable 'design-point' is selected on line A-B. Therefore, A-B is construed to be the locus of design points as well.

Line A-B is also plotted in Figs. 11 and 12 for a high side pressure up to 600 bar (600 bar is selected for completeness of the analysis). Optimal x_{op}, defined by the following expression is derived from Eq. 9,

$$x_{op} = \frac{\dot{m}_{HT,op}}{\dot{m}_{HT,op} + \dot{m}_{LT,op}} \tag{27}$$

The selected design point along this line provides information on the operational parameters of the WHR cycle, such as $p_1, p_2, \dot{m}_{HT,op}, \dot{m}_{LT,op}, \eta_{th}, \varepsilon$ and λ_{op}.

Figure 12 shows the variation of λ, ε and η_{th} of the WHR cycle along A-B. This figure discloses that the $\lambda_{op,max}, \varepsilon_{max}$ and $\eta_{th,max}$ are not coincident points. At $\lambda_{op,max}$, the product of ε and η_{th} is maximum. As explained earlier, higher compressor discharge pressures result in lower heat recovery effectiveness on account of higher discharge temperature, as shown in Fig. 12. One may note that the low side pressure variation is relatively small (96–114 bar) for a WHR cycle as it directly affects the output of both LT and HT turbines. In addition, since the enthalpy needed to drive the LT turbine in the DRDE WHR cycle is solely derived from the exhaust of the HT turbine, there is a tradeoff between the exhaust temperature and HT mass flow rate. This is the primary reason for the increase in split ratio (x) with the increase in compressor discharge pressure, as shown in Fig. 11.

Further extending the argument, the thermal efficiency initially increases up to 400 bar, similar to the trend reported for most sCO$_2$ cycles (Garg et al. 2013b) and thereafter, tends to decrease on account of increased compressor work at higher discharge pressure p_2 as observed from Fig. 12. Interestingly, as stated earlier, the heat recovery factor is

Fig. 11 Variation of λ_{op}, split ratio (x), and pressure ratio ($\frac{1}{p_r}$) with high side pressure along A-B
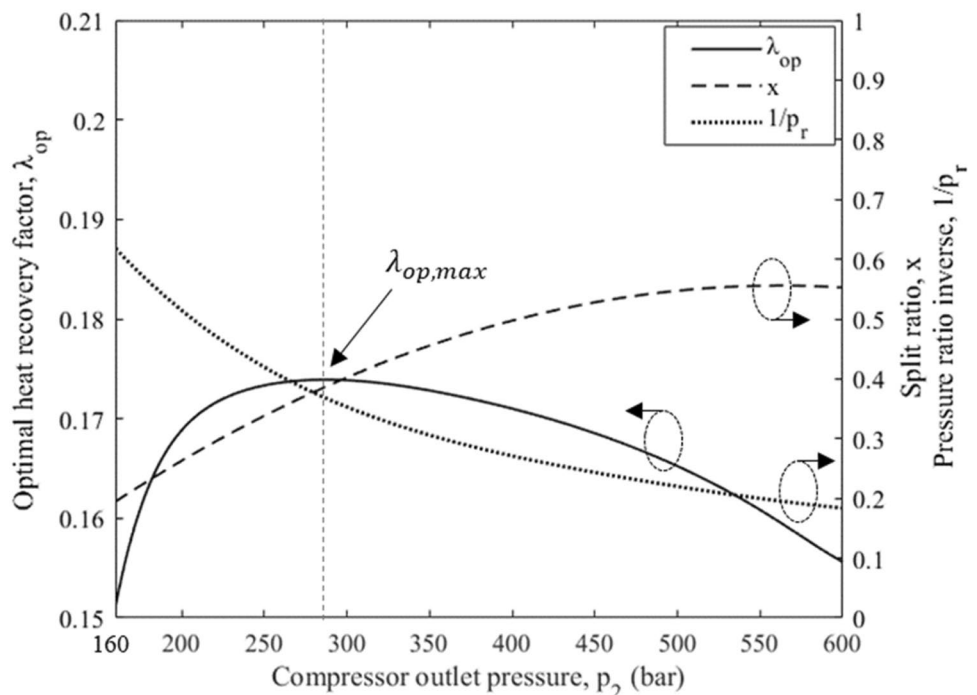
Fig. 12 Variation of λ, η_{th} and ε with high side pressure along A-B line
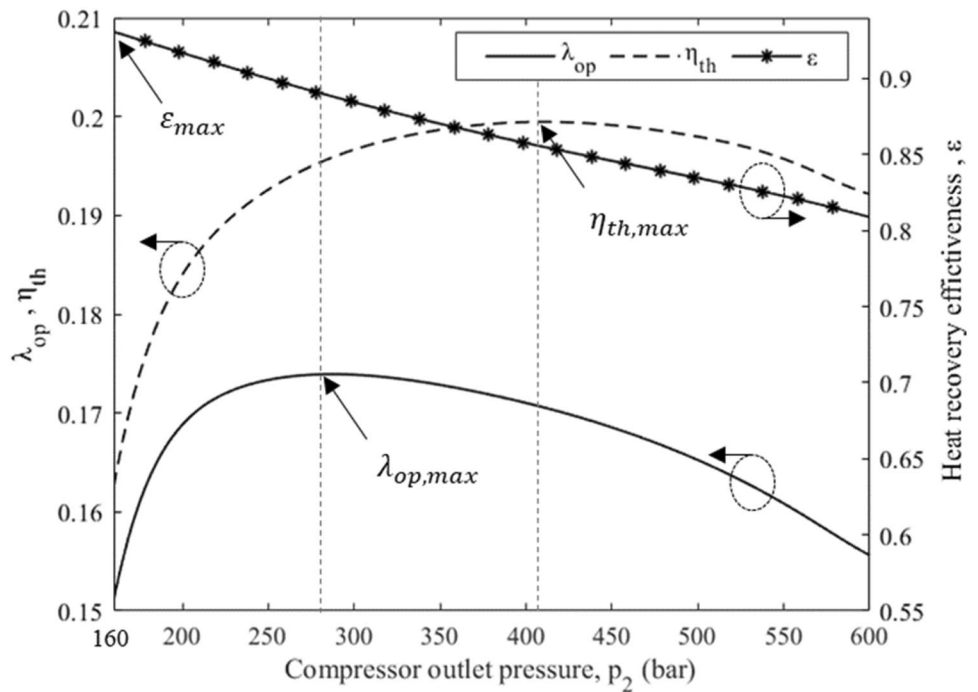

a tradeoff between effectiveness and cycle efficiency, and hence, the heat recovery factor attains a maximum at 280 bar corresponding to point A, shown in Figs. 7, 8, 9. Since the primary goal here is to maximize the work output, the suggested design-point for the WHR cycle is selected based on the maximum heat recovery factor. The corresponding

operating parameters and performance parameters based on the selected design-point 'A' arrived from the preceding assessment are summarized in Table 2.

The benefit of operating the WHR at the selected design point based on $\lambda_{op,max}$, corresponding high side pressure of 280 bar may not be viable from the perspective of plant

Fig. 13 Selection of economical design-point ($\lambda_{op,eco}$)
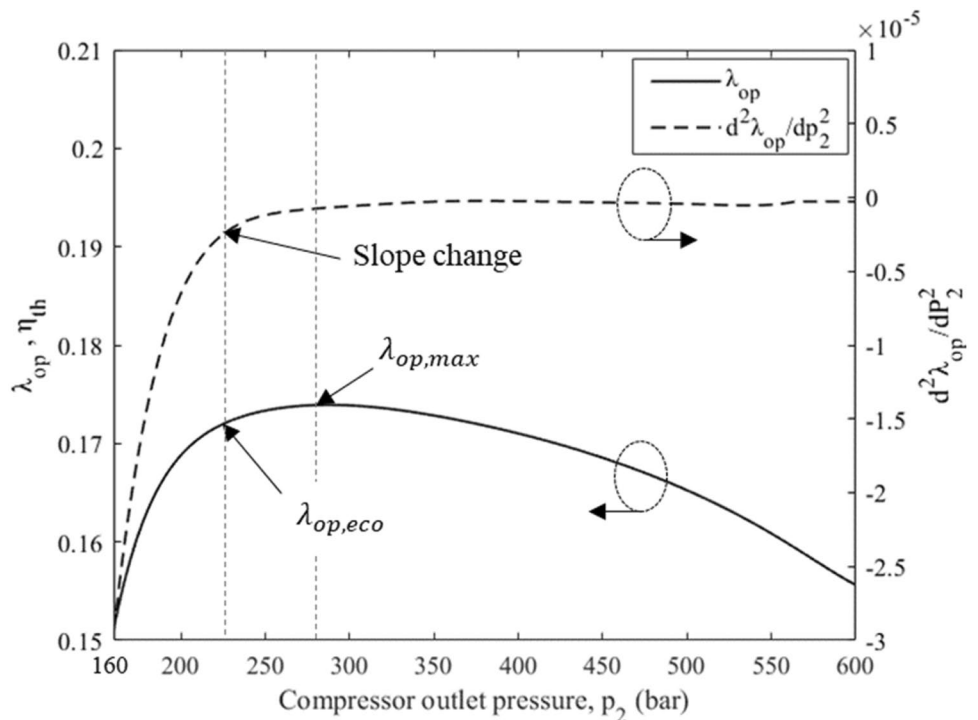
Table 2 WHR cycle design-point operating parameters

Compressor inlet pressure (p_1)(bar)	Compressor outlet pressure (p_2)(bar)	Pressure ratio ($\frac{1}{p_r}$)	Split ratio (x)	Heat recovery effectiveness (ε)	Cycle thermal efficiency (η_{th})	Heat recovery factor (λ)	$\frac{\dot{m}}{\dot{m}_{exh}}$
106	280	0.38	0.39	0.89	19.5%	17.4%	1.89

economics. Therefore, a balance between performance and cost needs to be made. Figure 13 helps in selecting an "economical" design-point vis-à-vis "preferred or optimal" design-point 'A.' A prudent selection of the design point is made by plotting the second derivative of the line A-B with respect to high side pressure as shown in the figure. The second derivative helps locate the point where the change of the slope of λ is maximum. For example, at $p_2 = 205$ bar, λ is 17%; and at $p_2 = 280$ bar, λ is 17.4%. An increase of 75 bar pressure in p_2 provides a meager increase of 0.4% in λ. Hence, the design-point in the vicinity of $p_2 \sim 220$ bar with $\lambda \sim 17.2\%$ is preferred from economic considerations.

Apart from cost benefits derived from lower operating pressures, reduction in compressor discharge pressure also facilitates a broader span of operation, thus reducing the associated anomalies of a stringent control system.

Effect of Isentropic Efficiencies of Turbomachines on WHR CYCLE Performance

The preceding analysis was based on fixed isentropic efficiencies of LT and HT turbines and compressor. Isentropic efficiency of the compressor and turbines was assumed to be 75% and 80%, respectively. It is well understood that isentropic efficiencies of the turbomachinery play a vital role in the performance of a power cycle. For an identical cycle pressure ratio, higher isentropic efficiency of the compressor leads to a lower outlet temperature, eventually resulting in higher heat recovery. This is in addition to lower power consumption by the compressor. Similarly, higher turbine isentropic efficiency provides more power and, thus, higher cycle efficiency. In summary, an increment in isentropic efficiency of either turbine or the compressor has a positive impact on the heat recovery factor of the WHR cycle.

Extending the line of thought, Fig. 14 shows the variation of optimum heat recovery factor (λ_{op}) along A-B with compressor discharge pressure for a range of isentropic efficiencies of both compressor and turbines. Line C-D, shown in the figure, is the locus of $\lambda_{op,max}$ points corresponding to the range of isentropic efficiencies investigated. One may observe that the optimal high side pressure (p_2), for the cycle increases with higher isentropic efficiency on account of lower discharge temperature at the compressor exit. A detailed investigation of the effect of turbomachinery

Fig. 14 Effect of turbomachine isentropic efficiencies on λ_{op} and allowable p_2
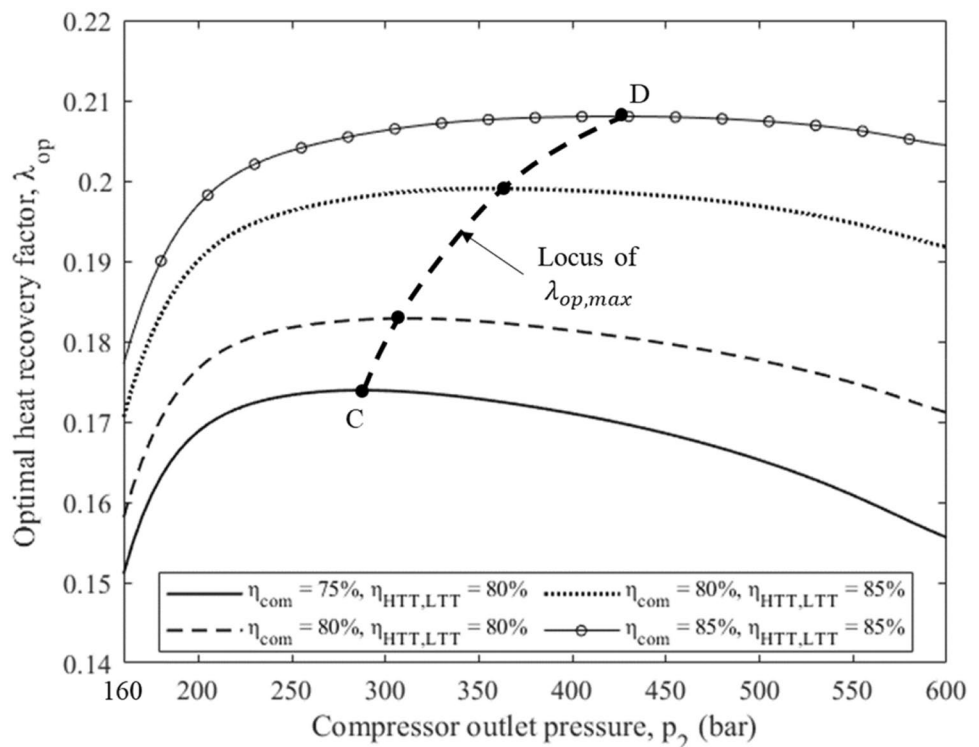
efficiency on plant economics and its influence on WHR operational variables is a separate study in itself and is not in the scope of the present paper.

Off-Design Performance Study

As with any power cycle, it is not possible to always operate the WHR cycle at its design point based on $\lambda_{op,max}$, with the parameters listed in Table 2. The off-design operation is significantly influenced not only by the off-design performance of the individual components but also by the cycle operating parameters. This section is dedicated to the off-design analysis of the WHR cycle, considering the effect of only the cycle operating parameters such as split ratio and pressure ratio. The analysis does not consider the off-design performance of the individual components like heat exchangers or turbomachinery.

Effect of Split Ratio

The definition of split ratio (x) is provided in Eq. 9. The effect of split ratio on WHR cycle heat recovery factor is shown in Fig. 15, keeping other parameters such as p_1, p_2 and total massflow rate $(\dot{m})$ fixed, as listed in Table 2.

Deviating from the optimal split ratio of $x_{op}= 0.39$, adversely impacts the heat recovery factor. The decrement in λ is more severe at suboptimal split ratios. A low split ratio would mean $\dot{m}_{HT} < \dot{m}_{HT,op}$, leading to lower heat

recovery effectiveness and thus, lower thermal efficiency. On the other hand, although increasing the split ratio does not impact the heat recovery effectiveness, both heat recovery factor and thermal efficiency drop on account of lower HT turbine inlet temperature. The effect of variation in optimum split ratio could be further aggravated if the off-design performances of the heat exchangers and turbomachinery were to be accounted for.

Effect of Operating Pressure Ratio

The operating pressure ratio (p_r) for the WHR cycle is defined in Eq. 16. The pressure ratio can be varied by varying either p_1 or p_2. The effect of pressure ratio on the WHR cycle heat recovery factor is shown in Fig. 16, keeping other parameters identical as listed in Table 2. In Fig. 16a, p_1 is varied keeping p_2 is fixed while in Fig. 16b, p_2 is varied keeping p_1 fixed.

Similar to the trend observed previously for varying split ratio, deviation from optimal design point pressure ratio of 0.38, on account of variation in either high side or low side pressures, adversely affects the WHR cycle performance. In both cases decreasing the pressure ratio positively impacts heat recovery effectiveness. However, at suboptimal pressure ratios, the influence of varying compressor inlet pressure p_1 is profound compared to varying p_2. Conversely, operating above the optimal pressure ratio has a nearly identical impact on heat recovery effectiveness. As explained previously, for the case of varying split

Fig. 15 Effect of split ratio on the WHR cycle performance
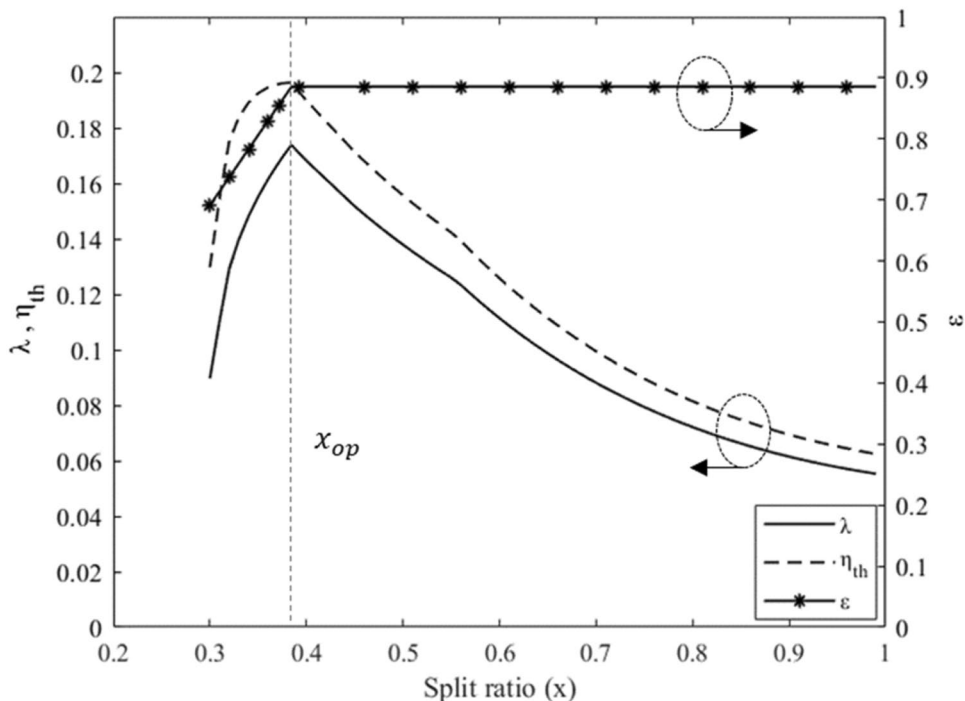
Fig. 16 Effect of pressure ratio on the WHR cycle performance. **a** p_2 fixed, **b** p_1 fixed
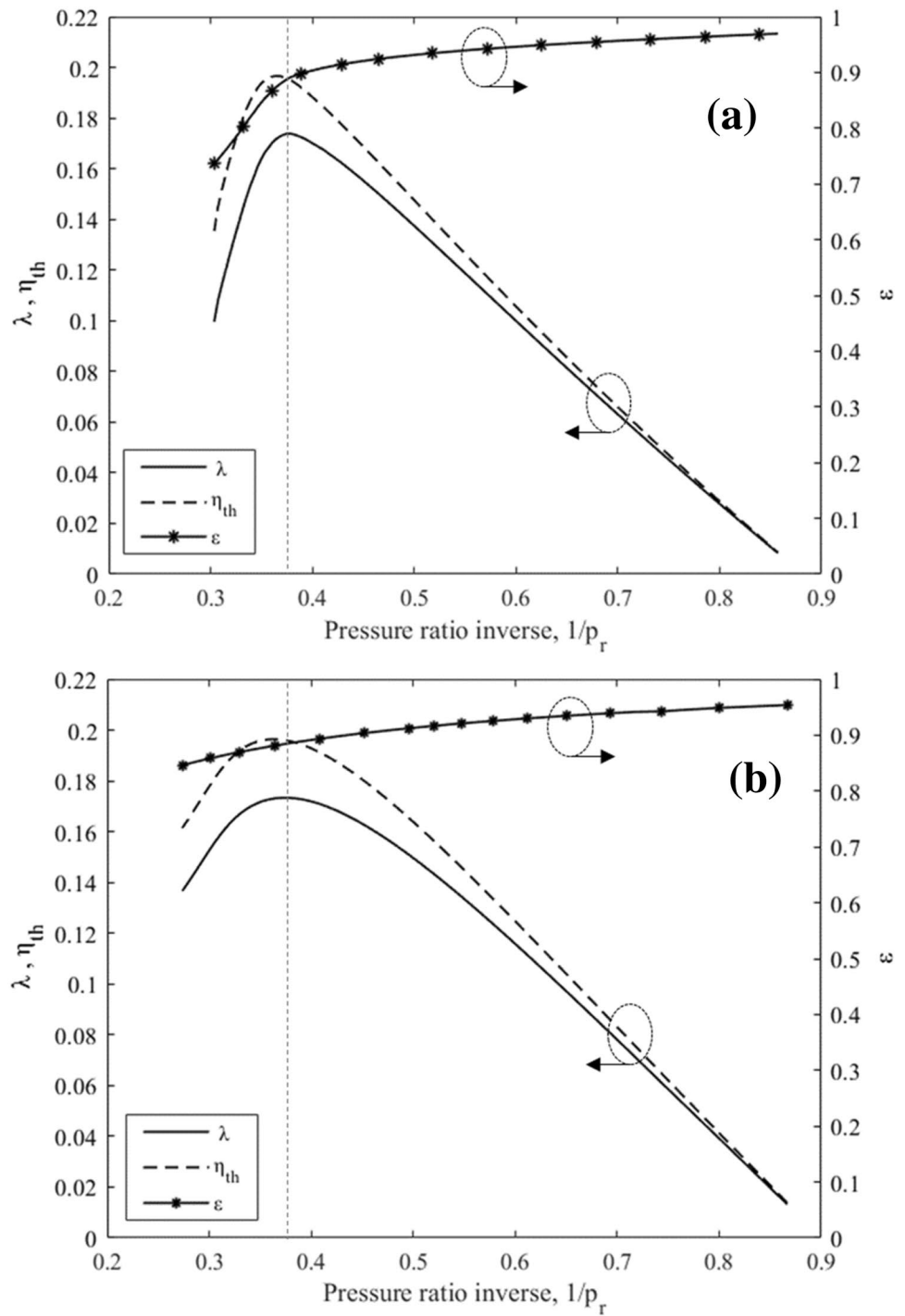

ratio, similar arguments hold good to explain the trend observed for both heat recovery factor and cycle efficiency with varying pressure ratios.

Comparison of Dual Recuperated Dual Expansion WHR Cycle with Baseline Single Recuperated sCO₂ Cycle

The schematic of the single recuperated sCO$_2$ cycle proposed for WHR application shown in Fig. 17 is the simplest and most common sCO$_2$ Brayton power cycles, which has been extensively investigated (Mohagheghi and Kapat

Fig. 17 Thermodynamic representation of single recuperated (SR) cycle
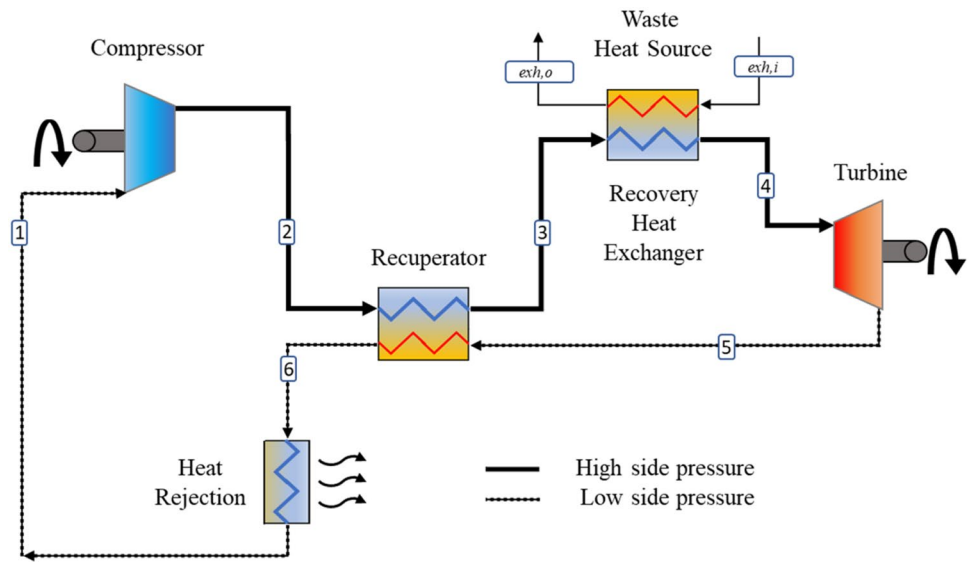
Fig. 18 Performance comparison between dual recuperated dual expansion (DRDE) and single recuperated (SR) cycle
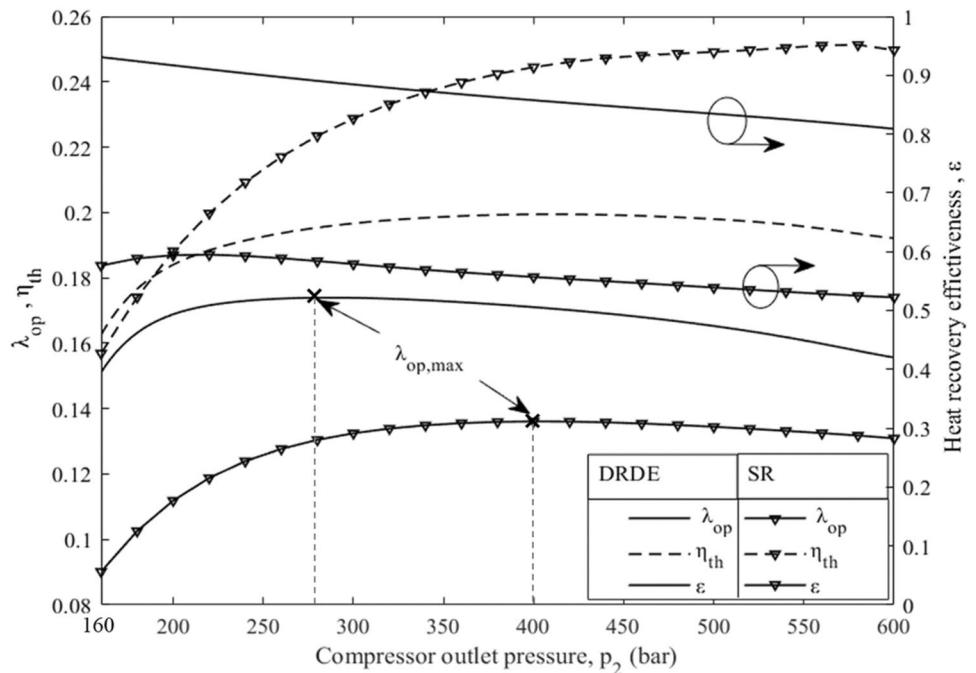
2013; Kimzey 2012; Cho et al. 2015; Wu 2016; Huck et al. 2016; Sen Wang, et al. 2018; Kim et al. 2016). From the point of view of plant economics, it is the most economical among all sCO_2 Brayton power cycles as it employs a single recuperator, a single turbine, and a single compressor. Considering this perspective, it is prudent to compare the performance of the present WHR cycle with the single recuperated cycle to derive the benefits (if any) in terms of net power output and other operational aspects.

For a fair comparison, the single recuperated cycle is subjected to a similar thermodynamic assessment considering identical operational parameters listed in Table 1.

The outcome of the analysis is summarized in Fig. 18. The performance of the current WHR cycle is also shown in Fig. 18. It is amply apparent that the heat recovery factor (λ) for the DRDE WHR cycle is significantly higher than the single recuperated (SR) cycle under all operating pressure ratios. The maximum value of heat recovery factor ($\lambda_{op,max}$) is 17.4% for the DRDE cycle compared to paltry 12.7%, for the SR cycle. Similarly, the optimal high side pressure (p_2) corresponding to $\lambda_{op,max}$ is 280 bar for DRDE WHR cycle compared to ~ 400 bar for the SR based WHR cycle. Higher operating pressure not only increases the plant cost but sometimes renders the plant impractical to operate.

An interesting aspect of the analysis presented in Fig. 18 is the significantly higher thermal efficiency (η_{th}) of the SR cycle, nearly 25% compared to 19.4% for the DRDE cycle. However, with increased cycle efficiency, the throughput from the SR cycle, indicated by the heat recovery factor (λ), is consistently lower compared to the DRDE cycle across all operating pressure ratios. It is mainly attributed to lower heat recovery effectiveness (ε) observed for the SR cycle. Maximum heat recovery effectiveness (ε) of the SR cycle is 0.55, compared to 0.88 for the DRDE cycle, corresponding to maximum heat recovery factor, $\lambda_{op,max}$. Poor heat recovery effectiveness offsets the benefit of higher cycle efficiency, putting the SR cycle at a disadvantage for a WHR application. In the SR cycle, the recuperator, which preheats the high-pressure sCO_2 from the compressor outlet using the turbine exhaust is primarily responsible for lower heat recovery from the waste heat source. In contrast, the DRDE cycle (shown in Fig. 2) does away with high-pressure recuperation, letting the high-pressure sCO_2 from the compressor outlet to be directly routed to the recovery heat exchanger, resulting in significantly higher heat recovery. Moreover, the inclusion of an additional recuperator further facilitates internal heat recovery, resulting in enhanced thermal efficiency.

Conclusions

This work presents a comprehensive analysis of a dual recuperated dual expansion sCO_2 based waste heat recovery cycle. The cycle parameters impacting the operational aspects of the DRDE-WHR cycle are lucidly obtained by reducing the number of variables from six to only four variables, viz. compressor inlet (p_1) and exit (p_2) pressures, HT ($\dot{m}_{HT}$) and LT ($\dot{m}_{LT}$) massflow rates. Subsequently, the influence of each parameter on the WHR cycle performance is systematically evaluated. The results are presented with air as the primary heat transfer fluid in the recovery heat exchanger for the WHR cycle shows an optimum split ratio of 0.39 at an operating pressure ratio of 0.38. These values correspond to a compressor outlet pressure of 280 bar for a waste heat source temperature of 500 °C. It is found that the heat recovery effectiveness (ε) for the WHR cycle is independent of $\dot{m}_{LT}$ and is mainly influenced by HT stream mass flow rate ($\dot{m}_{HT}$), high side pressure (p_2) and low side pressure (p_1). An important outcome of the paper is the influence of the heat recovery factor (λ) on the performance of the WHR cycle. The analysis shows that the heat recovery factor supersedes the thermal efficiency (η_{th}) for WHR applications. Optimal heat recovery factor (λ_{op}) is a product of thermal efficiency (η_{th}) and heat recovery effectiveness (ε) and does not coincide with the maxima of either of the two parameters. The extension of the study to off-design performance reveals that the DRDE-WHR is relatively inflexible

when it comes to varying either pressure ratio or the mass split fraction. Any deviation from the design point severely impairs the cycle performance, suggesting the requirement of a stringent control system.

Finally, a comparison with the baseline single recuperated sCO_2 cycle exhibits the superiority of the DRDE cycle, which consistently outperforms the single recuperated cycle across the entire range operating pressure ratio investigated. Although, the cycle thermal efficiency of the single recuperated sCO_2 is nearly 29% higher than the DRDE WHR cycle, the net power produced is 37% lower compared to the DRDE cycle on account of higher heat recovery by the DRDE cycle. This makes the DRDE cycle an ideal choice for WHR applications.

Appendix-I: Recovery heat exchanger pinch analysis

The design-point (point A) temperature profiles of the recovery heat exchanger in shown in Fig. 19. The hot (air) and cold (sCO_2) fluid stream temperatures vary across the heat exchanger's length with a pinch of 5 °C (minimum temperature difference between the hot and cold streams) occurring at both sides. Optimal HT massflow rate ensures this
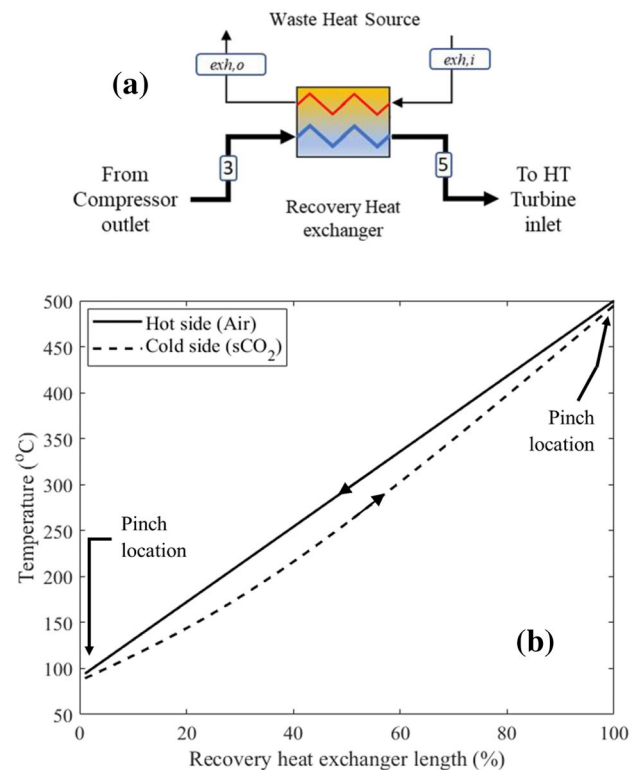
Fig. 19 Heat transfer in the waste heat heat-exchanger **a** Details of the recovery heat exchanger, **b** Temperature variation along the length across hot and cold streams

temperature distribution inside the heat exchanger. A lower HT massflow rate than the optimal value shifts the pinch location to the exhaust inlet (right) end. Similarly, A higher HT massflow rate than the optimal value shifts the pinch location to the sCO_2 inlet (left) end.

References

Ahn Y, Lee JI (2014) Study of various Brayton cycle designs for small modular sodium-cooled fast reactor. Nucl Eng Des. https://doi.org/10.1016/j.nucengdes.2014.05.032

Ahn Y et al (2015) Review of supercritical CO_2 power cycle technology and current status of research and development. Nucl Eng Technol 47(6):647–661. https://doi.org/10.1016/j.net.2015.06.009

Angelino G (1968) Carbon dioxide condensation cycles for power production. J Eng Gas Turbines Power. https://doi.org/10.1115/1.3609190

Cho SK, Kim M, Baik S, Ahn Y, Lee JI (2015) Investigation of the bottoming cycle for high efficiency combined cycle gas turbine system with supercritical carbon dioxide power cycle. https://doi.org/10.1115/GT2015-43077.

Dostal V, Driscoll MJ, Hejzlar P (2004) A supercritical carbon dioxide cycle for next generation nuclear reactors. Tech. Rep. MIT-ANP-TR-100

El Samad T, Teixeira JA, Oakey J (2020) Investigation of a radial turbine design for a utility-scale supercritical CO_2 power cycle. Appl Sci. https://doi.org/10.3390/APP10124168

Feher EG (1968) The supercritical thermodynamic power cycle. Energy Convers. https://doi.org/10.1016/0013-7480(68)90105-8

Forman C, Muritala IK, Pardemann R, Meyer B (2016) Estimating the global waste heat potential. Renew Sustain Energy Rev. https://doi.org/10.1016/j.rser.2015.12.192

Garg P, Kumar P, Srinivasan K, Dutta P (2013a) Evaluation of carbon dioxide blends with isopentane and propane as working fluids for organic Rankine cycles. Appl Therm Eng. https://doi.org/10.1016/j.applthermaleng.2012.11.032

Garg P, Kumar P, Srinivasan K (2013b) Supercritical carbon dioxide Brayton cycle for concentrated solar power. J Supercrit Fluids. https://doi.org/10.1016/j.supflu.2013.01.010

Garg P, Kumar P, Srinivasan K (2015) A trade-off between maxima in efficiency and specific work output of super- and transcritical CO_2 Brayton cycles. J Supercrit Fluids. https://doi.org/10.1016/j.supflu.2014.12.023

Held TJ (2015) Supercritical CO_2 cycles for gas turbine combined cycle power plants. Power Gen Int

Huck P, Freund S, Lehar M, Maxwell P (2016) Performance comparison of supercritical CO_2 versus steam bottoming cycles for gas turbine combined cycle applications

Incorvia C (2015) (12) United States Patent. 2(12): 1–4

Johnson GA, McDowell MW, O'Connor GM, Sonwane CG, Subbaraman G (2012) Supercritical CO_2 cycle development at pratt and whitney rocketdyne. https://doi.org/10.1115/GT2012-70105.

Khadse A, Blanchette L, Kapat J, Vasu S, Hossain J, Donazzolo A (2018) Optimization of supercritical CO_2 Brayton cycle for simple cycle gas turbines exhaust heat recovery using genetic algorithm. J Sol Energy Eng Trans ASME. https://doi.org/10.1115/1.4039446

Kim MS, Ahn Y, Kim B, Lee JI (2016) Study on the supercritical CO2 power cycles for landfill gas firing gas turbine bottoming cycle. Energy 111:893–909. https://doi.org/10.1016/j.energy.2016.06.014

Kimzey G (2012) Development of a brayton bottoming cycle using supercritical carbon dioxide as the working fluid. EPRI Rep: 1–31

Le Moullec Y (2013) Conceptual study of a high efficiency coal-fired power plant with CO_2 capture using a supercritical CO_2 Brayton cycle. Energy. https://doi.org/10.1016/j.energy.2012.10.022

Lee HJ, Kim H, Jang C (2014) Compatibility of candidate structural materials in high-temperature S-CO2 environment. In: 4th Int. Symp. - Supercrit. CO2 Power Cycles, pp. 1–9, 2014.

Lee J, Cho SK, Lee JI (2018) The effect of real gas approximations on S-CO_2 compressor design. J Turbomach. https://doi.org/10.1115/1.4038879

Lemmon EW, Huber ML, McLinden MO, et al. (2020) NIST standard reference database 23

Manente G, Costa M (2019) On the conceptual design of novel supercritical CO_2 power cycles for waste heat recovery. In: ECOS 2019 - Proc. 32nd Int. Conf. Effic. Cost, Optim. Simul. Environ. Impact Energy Syst., pp. 2219–2231

MATLAB (2020) version 7.10.0 (R2020a). Natick, Massachusetts: The MathWorks Inc.

Mohagheghi M, Kapat J (2013) Thermodynamic optimization of recuperated S-Co2 brayton cycles for waste heat recovery applications. In: 4th Int. Symp. - Supercrit. CO2 Power Cycles.

Moisseytsev A, Sienicki JJ (2009) Investigation of alternative layouts for the supercritical carbon dioxide Brayton cycle for a sodium-cooled fast reactor. Nucl Eng Des. https://doi.org/10.1016/j.nucengdes.2009.03.017

Neises T, Turchi C (2014) A comparison of supercritical carbon dioxide power cycle configurations with an emphasis on CSP applications. https://doi.org/10.1016/j.egypro.2014.03.128.

Olumayegun O, Wang M (2019) Dynamic modelling and control of supercritical CO_2 power cycle using waste heat from industrial processes. Fuel. https://doi.org/10.1016/j.fuel.2019.03.078

Pandey V, Kumar P, Dutta P (2020) Thermo-hydraulic analysis of compact heat exchanger for a simple recuperated sCO_2 Brayton cycle. Renew Sustain Energy Rev. https://doi.org/10.1016/j.rser.2020.110091

Papapetrou M, Kosmadakis G, Cipollina A, La Commare U, Micale G (2018) Industrial waste heat: estimation of the technically available resource in the EU per industrial sector, temperature level and country. Appl Therm Eng. https://doi.org/10.1016/j.applthermaleng.2018.04.043

Qi J, Reddell T, Qin K, Hooman K, Jahn IHJ (2017) Supercritical CO_2 radial turbine design performance as a function of turbine size parameters. J Turbomach. https://doi.org/10.1115/1.4035920

Sathish S, Kumar P, Nassar A (2021) Analysis of a 10 MW recompression supercritical carbon dioxide cycle for tropical climatic conditions. Appl Therm Eng. https://doi.org/10.1016/j.applthermaleng.2020.116499

Sen Wang S, Wu C, Li J (2018) Exergoeconomic analysis and optimization of single-pressure single-stage and multi-stage CO_2 transcritical power cycles for engine waste heat recovery: a comparative study. Energy. https://doi.org/10.1016/j.energy.2017.10.055

Us OH (2013) Supercritical carbon dioxide power cycle for waste heat recovery. 2(12). [Online]. Available: https://google.com/patent/US9341084B2/en.

Vance D et al (2019) Estimation of and barriers to waste heat recovery from harsh environments in industrial processes. J Clean Prod. https://doi.org/10.1016/j.jclepro.2019.03.011

Wu C et al (2016) System optimisation and performance analysis of CO2 transcritical power cycle for waste heat recovery. Energy. https://doi.org/10.1016/j.energy.2015.12.001

Xia L, Li X, Song J, Ren X, Gu C (2019) Design and analysis of S-CO_2 Cycle and radial turbine for SOFC vehicle waste-heat recovery. J Therm Sci. https://doi.org/10.1007/s11630-019-1105-9

Yoon HJ, Ahn Y, Lee JI, Addad Y (2012) Potential advantages of coupling supercritical CO_2 Brayton cycle to water cooled small and medium size reactor. Nucl Eng Des. https://doi.org/10.1016/j.nucengdes.2012.01.014

Publisher's Note Springer Nature remains neutral with regard to jurisdictional claims in published maps and institutional affiliations.